SCIENCE CHINA Materials ARTICLES

mater.scichina.com link.springer.com

Published online 4 April 2018 | https://doi.org/10.1007/s40843-017-9237-2
Sci China Mater 2018, 61(6): 895–904

SPECIAL ISSUE: Advanced Materials for Photoelectrochemical Cells

A dual-electrolyte system for photoelectrochemical hydrogen generation using $CuInS_2$-In_2O_3-TiO_2 nanotube array thin film

Charlene Ng, Jung-Ho Yun, Hui Ling Tan, Hao Wu, Rose Amal and Yun Hau Ng*

ABSTRACT **The utilization of Na_2S/Na_2SO_3 mixture as the electrolyte solution to stabilize sulfide anode in a photoelectrochemical cell for hydrogen evolution generally compromises the current-to-hydrogen efficiency ($\eta_{current}$) of the system. Here, the employment of a dual-electrolyte system, that is, Na_2S/Na_2SO_3 mixture and pH-neutral Na_2SO_4 as the respective electrolyte solutions in the anode and cathode chambers of a water splitting cell is demonstrated to suppress the photocorrosion of $CuInS_2$-In_2O_3-TiO_2 nanotube (CIS-In_2O_3-TNT) heterostructure, while simultaneously boosts the $\eta_{current}$. Although n-type CIS and In_2O_3 nanoparticles can be easily formed on TNT array *via* facile pulse-assisted electrodeposition method, conformal deposition of the nanoparticles homogeneously on the nanotubes wall with preservation of the TNT hollow structure is shown to be essential for achieving efficient charge generation and separation within the heterostructure. In comparison to Na_2S/Na_2SO_3 solution as the sole electrolyte in both the anode and cathode chambers, introduction of dual electrolyte is shown to not only enhance the photostability of the CIS-In_2O_3-TNT anode, but also lead to near-unity $\eta_{current}$ as opposed to the merely 20% $\eta_{current}$ of the single-electrolyte system.**

Keywords: dual-electrolyte, hydrogen generation, photoelectrochemical, TiO_2 nanotubes, $CuInS_2$

INTRODUCTION

Photoelectrochemical hydrogen (H_2) generation using light-driven semiconductor electrodes is an attractive way for converting solar energy to chemical energy [1]. H_2 evolved from the photoelectrolytic cleavage of water or the photodecomposition of organic waste has been achieved [2]. While titanium dioxide (TiO_2) traditionally is a promising candidate in this application [3], continuous improvements of its light absorption and charge transport properties are under vigorous investigation as TiO_2 is held back by its wide optical bandgap and rapid charge recombination [4]. Strategies for improving these limitations include (i) doping with metallic or non-metallic elements to narrow its optical bandgap [5], (ii) nanostructuring to improve charge separation and transportation (e.g., development of low dimensional structure for directional electron flow) [6], (iii) introducing secondary component of smaller bandgap energy to extend the light absorption to visible region [5] and (iv) crystal facet engineering to tailor the exposure extent of more reactive facets [7,8].

The efficacy of the combination of strategies (ii) and (iii) was previously demonstrated to fabricate a p-n heterojunction photoelectrode comprising p-type $CuInS_2$ (CIS) nanoparticles conformally deposited on both the outer and inner walls of one-dimensional well-aligned n-type TiO_2 nanotube (TNT) array, which showed promising photodiode behavior and enhanced visible light-triggered photoelectrochemical photocurrent [3]. In liquid junction photoelectrochemical cells for H_2 generation, however, the band energy alignment of a composite photoanode would prefer the construction of all n-type heterojunction photoactive semiconductors. CIS is an interesting copper-based chalcopyrite with flexibility in exhibiting either p-type or n-type semiconductor behavior upon manipulation of copper vacancies in the crystal structure [9]. Following on our study that showed tunable CIS carrier type through the control of $CuCl_2$:$InCl_3$:

Particles and Catalysis Research Group, School of Chemical Engineering, The University of New South Wales, UNSW Sydney 2052, Australia
* Corresponding author (email: yh.ng@unsw.edu.au)

$Na_2S_2O_3$ ratio in the precursor solution [3], herein a new n-type composite photoanode comprising TNT array (3.2 eV), In_2O_3 (2.8 eV) and CIS (1.5 eV) is designed *via* the pulse-assisted electrodeposition approach. With this configuration, a wider light spectrum can be readily absorbed by the relevant component with suitable optical bandgap.

Modification of wide bandgap oxide semiconductor with CIS offers opportunities in enhancing the photon absorption and charge transport. Despite having advantages such as high absorption coefficient (10^5 cm^{-1}, which indicates thickness of only 1–2 μm is sufficient to absorb most of the light) and narrow bandgap, the chemical instability of CIS due to photocorrosion or depletion of sulfur imposes challenges in handling it in liquid phase [10]. Most literatures reported the use of reducing agent (i.e., hole scavenger) to stabilize CIS during illumination, whereby the photogenerated holes in CIS are scavenged to prevent its self-oxidation. The reducing agents generally employed for sulfide materials include sulfide (S^{2-}), sulfite (SO_3^{2-}) and thiosulfate ($S_2O_3^{2-}$) ions. Although S^{2-} ions were demonstrated to have the strongest hole-scavenging ability [11], addition of SO_3^{2-} ions was found useful to suppress the formation of the undesirable disulfide (S_2^{2-}) ions [12]. Mixture of S^{2-} and SO_3^{2-} is therefore more favorably used to stabilize sulfide materials and has widely shown to perform effectively in powder-type photocatalytic H_2 production [12,13]. However, in a photoelectrochemical system which involves the shuttling of photogenerated electrons from the anode to cathode, the utilization of electrons at the cathode is a competitive reaction between the reduction of H^+ to H_2 and the reduction of $S_2O_3^{2-}$ to S^{2-} and SO_3^{2-}. Although increased photocurrent generation is observed attributing to the improved stability of sulfide photoanode, poor current-to-hydrogen efficiency ($\eta_{current}$) is generally yielded due to the competing reduction reactions at the cathode.

Herein, we report the construction of a dual-electrolyte system which employed a mixture of Na_2S and Na_2SO_3 (Na_2S/Na_2SO_3) as the model reducing agent for stabilizing the chalcopyrite-containing photoanode (CIS-In_2O_3-TNT), while using a typical pH-neutral Na_2SO_4 electrolyte in the cathode chamber to achieve greater $\eta_{current}$. To the best of our knowledge, this is the first successful attempt to overcome both the stability and $\eta_{current}$ issues associated with chalcopyrite photoanode *via* a dual electrolyte system, in which this strategy should potentially provide solutions to challenges associated with photoelectrochemical cells design.

EXPERIMENTAL DETAILS

Anodized TNT arrays

The TNT array was prepared by anodizing Ti foil (99.7%, Aldrich) with 20×20×0.127 mm dimension in ethylene glycol based fluoride electrolyte. The Ti foils were first cleaned with acetone in mild sonication and Milli-Q water followed by vacuum drying before anodization. The electrolytes were prepared by mixing ethylene glycol (>99%, Aldrich) and 0.5 wt.% of NaF (99%, Ajax Chemicals) with water of 5 wt.%. A two-electrode system was used for anodization, with Ti foil as the anode, and platinum plate and wire as the cathode. An in-house designed sealed anodic cell was used as the reactor. A constant distance was maintained between electrodes, and the area of anode exposed to the electrolyte was controlled. A programmable direct current (DC) power supply (PST-3201, GW Instek) interfaced with a computer was used to monitor the anodization current density. Anodization was performed at the applied potential of 60 V with different anodizing durations of 1, 3 and 7 h. After anodization, the TNT array samples were rinsed with Milli-Q water in a sonication bath to remove debris of broken tubes, and dried at 110°C for 1 h, followed by calcination at 450°C for 3 h with a ramping rate of 5°C min^{-1} in air.

CIS-TNT composites

To fabricate CIS-TNT photoelectrode, prior to deposition of CIS onto the TNT, the calcined TNT array was placed in the sealed anodic cell, in which the CIS was deposited electrochemically by applying a square pulse with a switch to a cathodic pulse (−1.2 V, 200 ms) and short circuit pulse (0 V, 200 ms); the pulse was employed by a function generator (TG4001, Thurlby Thandar Instruments). For n-type CIS, In-rich CIS precursor solution was prepared with $CuCl_2$, $InCl_3$, and $Na_2S_2O_3$ in molar ratio of 3:7:50. After CIS deposition, the CIS-TNT array samples were annealed at 500°C for 1 h with ramping rate of 5°C min^{-1} in a tube furnace under Ar. The samples are abbreviated by the composite and anodizing duration of the TNT array; CIS-In_2O_3-TNT1, CIS-In_2O_3-TNT3 and CIS-In_2O_3-TNT7 correspond to the products obtained from pulsed-electrodeposition treatment on the TNT arrays anodized for 1, 3 and 7 h, respectively.

Material characterizations

The crystal phases of TNT and CIS-In_2O_3-TNT composite films were obtained on an X-ray diffractometer (Xpert Pro MRD, Philips). The morphologies of all samples were

investigated using a scanning electron microscope (SEM, S900, Hitachi). The optical bandgap energies of the CIS-In_2O_3-TNT composite films were analyzed using a diffuse reflectance UV spectrophotometer (Cary 300, Varian). The amperometry measurements were performed in an aqueous solution containing 0.25 mol L^{-1} of Na_2S and 0.35 mol L^{-1} of Na_2SO_3 using a potentiostat (PG STAT-302N, Autolab, applied bias 0.75 V) in a standard three-electrode system comprising TNT or CIS-In_2O_3-TNT composite film as the working electrode, Ag/AgCl as the reference electrode and Pt as the counter electrode. Prior to measurement, the electrolyte was purged with Ar for 10 min. A 300 W Xe lamp coupled with 435 nm cutoff filter was the visible light source.

Photoelectrochemical water splitting reaction

The water splitting reaction was carried out with an applied bias of 1.0 V in a two-electrode cell with CIS-In_2O_3-TNT1 as the working electrode and Pt as the counter electrode, which were placed separately in two chambers connected with a Nafion membrane. An aqueous solution containing a mixture of 0.25 mol L^{-1} of Na_2S and 0.35 mol L^{-1} of Na_2SO_3 at pH 12 or 0.5 mol L^{-1} of Na_2SO_4 was used as the electrolyte in both chambers. For the dual-electrolyte system, the 0.25 mol L^{-1} of Na_2S and 0.35 mol L^{-1} of Na_2SO_3 mixture was employed as the electrolyte solution in the anode chamber, while 0.5 mol L^{-1} of Na_2SO_4 in the cathode chamber. The system was purged with Ar (main carrier gas of the system) for 1 h prior to illumination with visible light ($\lambda \geq 435$ nm) from a 300 W Xe lamp. The evolved H_2 gas was quantified using a gas chromatography (GC-8A, Shimadzu).

RESULTS AND DISCUSSION

Given that Cu and In-rich precursor solutions were demonstrated to yield CIS with p and n-type characters, respectively [3], an In-rich precursor solution was thus employed in this work to pulsed-electrodeposit n-type CIS nanoparticles on the surfaces of the TNT array to yield all n-type CIS-TNT heterojunction photoanode. Prior to the pulsed-electrodeposition treatment, three vertically aligned TNT arrays with distinct tube lengths were prepared using different anodizing durations, namely TNT1, TNT3 and TNT7 represent the respective samples obtained with 1, 3 and 7 h of anodization. Cross-sectional imaging of the TNT samples under SEM manifests that the length of the TNT arrays increases from 3.3 μm for TNT1, to 10.5 μm for TNT2 and 13.8 μm for TNT3, indicating that the nanotube length is proportional to the anodizing time as reported previously [14].

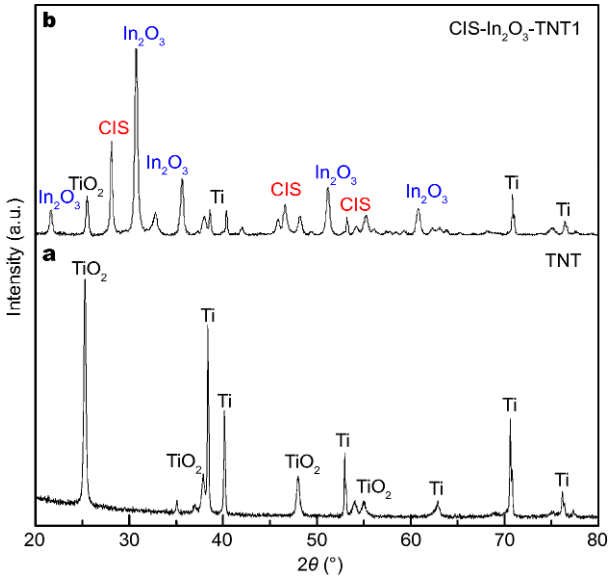

Figure 1 XRD spectra of CIS-In_2O_3-TNT1 and TNT1 anodized for 1 h.

The crystal phase of all TNT samples was found to be similar, as determined using X-ray diffraction (XRD) analysis. The XRD pattern of TNT1 (Fig. 1a) is therefore taken as a representative of all the TNT samples. The three prevalent peaks at 25.4°, 38.1° and 48.2°, which correspond to the (101), (004) and (200) planes of anatase TiO_2, respectively, confirm that all TNT samples are anatase phase. The discernible Ti-related peaks are attributed to the Ti foil substrate, on which the top section was transformed into TNT array *via* anodization.

In addition to the TiO_2 and Ti peaks as exhibited by the TNT array, the peaks associated with tetragonal CIS and cubic In_2O_3 are also exhibited by all TNT arrays subjected to pulsed-electrodeposition treatment in the CIS precursor-containing aqueous solution, as represented by the XRD pattern of the CIS-adorned TNT1 sample in Fig. 1b. The relatively low intensity of the TiO_2 and Ti peaks suggests the successful deposition of CIS on the TNT arrays with the presence of In_2O_3 impurity, confirming the formation of composite electrodes consisting of CIS, In_2O_3 and TNT with different nanotube lengths. Formation of In_2O_3 in Cu-In-VI_2 chalcopyrite has generally been attributed to thermal oxidation of the material *via* post-annealing treatment in O_2-containing atmosphere [15,16]. The possibility of In_2O_3 formation predominantly during the annealing post-treatment in this study, however, could be eliminated since the treatment was done in O_2-deficient Argon environment. Instead, the In_2O_3 could be concomitantly generated during pulsed-electro-

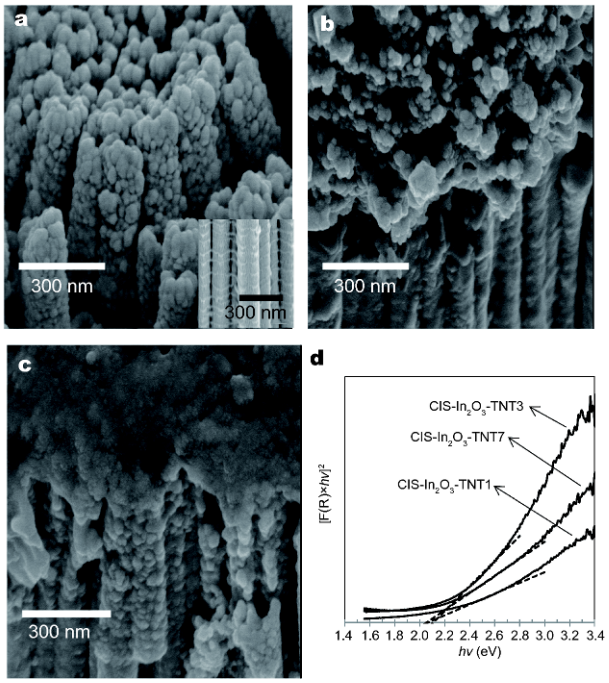

Figure 2 SEM images of (a) CIS-In_2O_3-TNT1, (b) CIS-In_2O_3-TNT3, (c) CIS-In_2O_3-TNT7 and (d) UV-vis diffuse reflectance spectra of the CIS-In_2O_3-TNT heterostructures. The inset in (a) presents the SEM image of TNT1.

deposition of CIS on the TNT arrays. While further experiment is needed to elucidate the actual formation pathways of the In_2O_3 in this synthetic method, the possible routes could be (i) reduction of O_2 present in the CIS precursor solution by the S^{2-} anions and followed by chemical reaction between O_2 and In^{3+} cations and/or (ii) direct formation of In_2O_3 as corroborated by the highly positive reduction potential of the reaction (Equation 1) [17].

$$1.5O_2 + 2In^{3+} + 6e^- \rightarrow In_2O_3 \ (E^0 = 1.09\ \text{V}). \quad (1)$$

The relatively higher intensity of In_2O_3 in comparison to that of CIS in all the composite electrodes can be attributed to the utilization of In-rich precursor solution during the pulsed-electrodeposition process, in which the presence of high amount In^{3+} favors In_2O_3 formation.

SEM was employed to investigate the deposition quality of CIS/In_2O_3 on the TNT arrays of different nanotube lengths after pulsed-electrodeposition under the same experimental conditions. The inset in Fig. 2a displays the representative SEM image of the TNT array, which is utilized as the substrate for CIS deposition, is composed of highly ordered and vertically oriented nanotubes. After the pulsed-electrodeposition process, the top and outer walls of the CIS-In_2O_3-TNT1 are homogenously covered by CIS/In_2O_3 nanoparticles without any closure of the tubes (Fig. 2a). As discussed in our previous work, the key to the successful coating of nanoparticles is the relaxation time introduced during electrodeposition [3]. The continuous pulse-assisted approach allows the creation of nucleation sites under a high cathodic voltage of −2 V (200 ms) and diffusion of precursor to the sites situated deeper into the nanotubes during the 200 ms relaxation time at 0 V. Furthermore, the relaxation pulse also enhances uniform nucleation of particles on the walls of TNT through homogenous diffusion over the TNT.

However, the deposition of these particles is shown to be dependent on the lengths of the TNT arrays, as depicted in Fig. 2b, c. Although homogenous deposition of the CIS/In_2O_3 nanoparticles is observed on the outer wall of the longer TNT arrays (CIS-In_2O_3-TNT3 and CIS-In_2O_3-TNT7), a large amount of CIS/In_2O_3 nanoparticles are also found deposited on top of the nanotubes that leads to tube closure. For CIS-In_2O_3-TNT3, a layer of agglomerated nanoparticles is apparent on top of the tubes, whereas a compact layer of sintered CIS/In_2O_3 particles is observed on the TNT7 array which has the longest nanotube length. The accumulation of these deposited nanoparticles is analogous to the continuous electrodeposition of CIS without a relaxation time as shown in our previous work [3]. These results then indicate that the extensive deposition of CIS/In_2O_3 nanoparticles on the top of CIS-In_2O_3-TNT3 and CIS-In_2O_3-TNT7 is associated with the insufficient relaxation time provided during the pulsed-electrodeposition process. The inadequate relaxation time prevents the CIS precursor from reaching the nucleation sites situated at a much greater depth of the longer nanotubes, causing inhomogeneous growth of CIS/In_2O_3 particularly on top of the nanotubes and the accumulation of nanoparticles results in the subsequent closure of the tubes. The findings suggest that the longer nanotube length, the larger the amount of CIS/In_2O_3 nanoparticles being deposited on the top of TNT array and thus the faster the closure of the nanotubes.

The optical properties of all the CIS-In_2O_3-TNT composite films were determined using UV-vis spectroscopy. According to the Kubelka-Munk plots in Fig. 2d, a comparable optical band gap of 2.1 eV can be estimated for all the composites, indicating their ability to respond under visible light irradiation. Since TiO_2 has large band gap energy of 3.2 eV, the extended absorbance in the visible light region is essentially attributed to the deposited CIS and In_2O_3 particles. Due to the composite nature of the film, the resulting optical band gap lies in

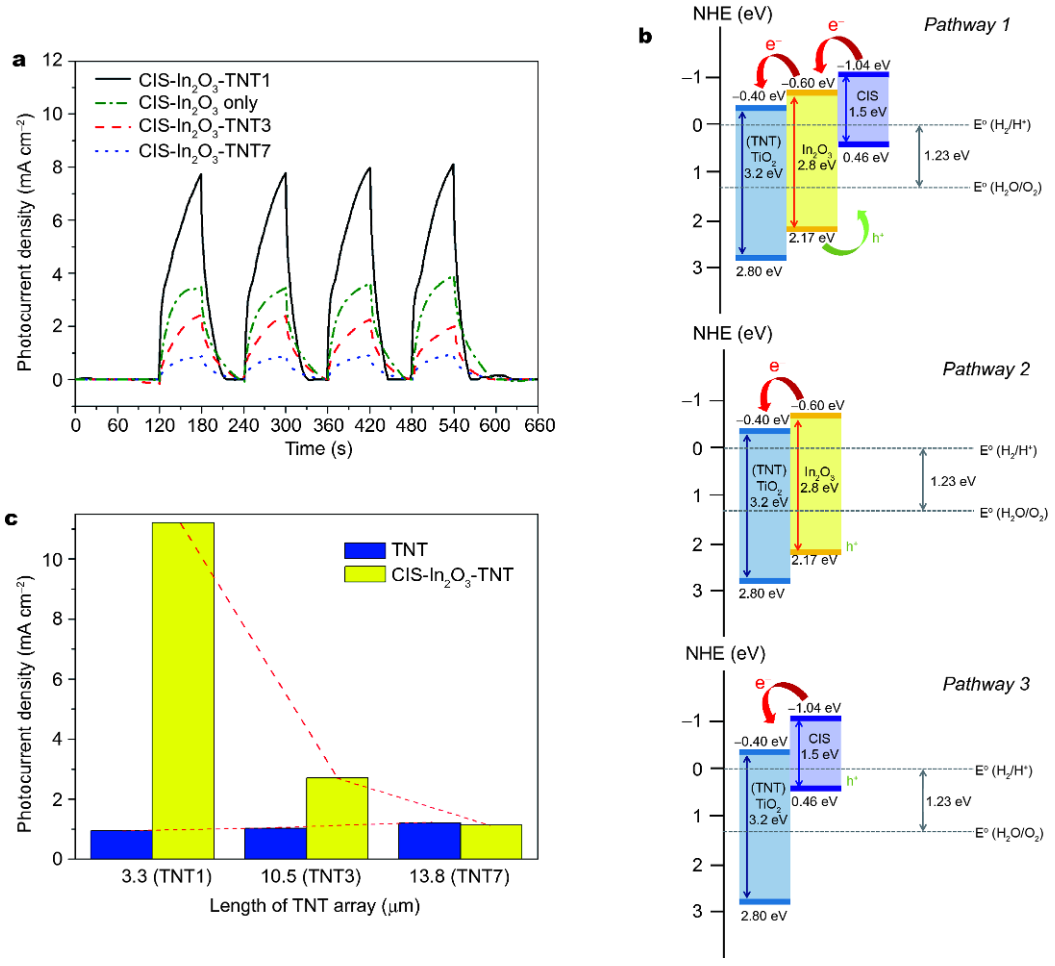

Figure 3 (a) Amperometric photocurrent densities of CIS-In_2O_3 and CIS-In_2O_3-TNT arrays with different lengths of TNT arrays under visible light irradiation (λ>435 nm) in Na_2S/Na_2SO_3 electrolyte solution. (b) Schematic diagram on energy band gap and different photoexcited electron pathways within the CIS-In_2O_3-TNT composite photoelectrode. (c) Photocurrent density comparison of the TNT arrays and CIS-In_2O_3-TNT electrodes with different lengths under UV illumination.

between the band gap energy of CIS (1.5 eV) and In_2O_3 (2.8 eV) particles.

The photoactivities of the CIS-In_2O_3-TNT composites with distinct nanotube lengths and CIS/In_2O_3 deposition quality were compared by measuring their photoresponses on a standard three-electrode photoelectrochemical system comprising the composite film as the working electrode, Ag/AgCl as the reference electrode and platinum (Pt) foil as the counter electrode. All of the photocurrent responses show anodic photocurrent, indicating that the fabricated CIS-In_2O_3-TNT electrodes are n-type semiconductor. Owing to the large band gap energy of approximately 3.2 eV, negligible photocurrent was generated by all bare TNT arrays under visible light ($\lambda \geq$ 435 nm). However, incorporation of CIS and In_2O_3 *via* pulse-assisted electrodeposition approach evidently enhances the visible-light-triggered photoresponses of the TNT arrays, as exhibited in Fig. 3a. The improved photoresponses of CIS-In_2O_3-TNT composite films under visible light irradiation is attributed to the presence of the visible-light-active CIS and In_2O_3, which both act as the primary light absorbers while the TNT arrays function as the electron conductor. Given that the conduction band of TiO_2 is located at −0.40 V (*vs.* normal hydrogen electrode (NHE)), which is more anodic than the conduction bands of CIS (−1.04 eV *vs.* NHE) and In_2O_3 (−0.60 eV *vs.* NHE), the suitable band alignments of these components favor electron injection from CIS and In_2O_3 to the TNT array. Upon visible light illumination, the excited electrons within CIS and In_2O_3 can be injected into TNT in 3 different pathways as illustrated in Fig. 3b. When both CIS and In_2O_3 are in sequential contact with TNT, the

excited charges can be injected consecutively *via* pathway 1 from the CIS to In_2O_3 and eventually to TNT, as a result of the suitable band position of CIS and In_2O_3. In the second and third pathway, the TNT can exclusively accept electrons from either CIS or In_2O_3. These thermodynamically feasible charge transfer band alignments can reduce the recombination of excited charges within CIS and In_2O_3, resulting in the enhanced photoresponses of the composite films. In addition to the appropriate band positions, the vectorial charge conductance pathway provided by the geometrical architecture of the one-dimensional TNT also assists in charge separation within the composite, at which electrons are transported along the nanotube axis to the Ti conducting substrate and holes move radially outward to the nanotube surface [18,19].

Note that CIS-In_2O_3-TNT1 unambiguously showed the highest photocurrent of 7.7 mA cm^{-2} (Fig. 3a), which can be attributed to the homogeneous and conformal deposition of CIS/In_2O_3 nanoparticles on the surfaces of the TNT1 array without sealing the tubes. The tubular channels function as the light scattering centers within the film to increase the light absorption and allow sensitization of the CIS/In_2O_3 present deep into the nanotubes [20], rendering efficient charge generation and separation within CIS-In_2O_3-TNT1. In contrast, abundant deposition of CIS/In_2O_3 nanoparticles on the top of TNT3 and TNT7 arrays seals the nanotubes and hence restricts light penetration to reach the CIS and In_2O_3 components that are underneath the dense CIS/In_2O_3 layer and directly deposited on the nanotubes wall. Since only the near surface CIS/In_2O_3 sitting on the top of TNT arrays can be excited, the photogenerated electrons have to diffuse a long distance through the thick blocking layer of nanoparticles enriched with recombination sites and then along the TNT to reach the Ti foil, which reduces the number of electrons that can be extracted from the CIS-In_2O_3-TNT3 and CIS-In_2O_3-TNT7 electrodes, as verified by their considerably poor photocurrents. In such cases, instead of functioning as scattering centers, the presence of the sealed-end TNT arrays impedes electron transfer from the CIS/In_2O_3 layer to the charge collecting Ti foil. This is evinced by the superior performance of CIS-In_2O_3 electrode, which was prepared by pulsed-electrodeposition of CIS onto Ti foil without the presence of TNT array. In the absence of TNT array, excitation of CIS-In_2O_3 layer deposited directly on the Ti foil produced higher photocurrent than both the CIS-In_2O_3-TNT3 and CIS-In_2O_3-TNT7 electrodes.

In order to delve into the influence of TNT length towards the overall CIS-In_2O_3-TNT photocurrent performance, the photoelectrochemical measurements were repeated under UV illumination since TiO_2 was only active under UV light. The photocurrent responses of the bare TNT arrays with different lengths were measured for control purposes. As shown in Fig. 3c, the photocurrent responses of these bare TNT arrays rise gradually from 0.9 to 1.2 mA cm^{-2} as the TNT length increases, while the photocurrent densities of the CIS-In_2O_3-TNT electrodes decline as the length of the TNT array increases. Interestingly, the CIS-In_2O_3-TNT3 and CIS-In_2O_3-TNT7 photoanodes exhibit similar photoresponse under both visible light and UV illumination. The comparable magnitude of photocurrent indicates that the CIS/In_2O_3 dense layer on the surfaces of the materials efficiently blocks the light from penetrating and activating the TNT arrays. On the other hand, the performance trend of the composite films under UV illumination concurs with that under visible light, that is, CIS-In_2O_3-TNT1 > CIS-In_2O_3-TNT3 > CIS-In_2O_3-TNT7. In spite of the improved photocurrent of the bare TNT array with longer nanotube length under UV light, the analogous decline in the photoactivities of the composite films with the increase of TNT length under both visible and UV irradiations indicates that the TNT length does not play a role in governing the performances of the composite films. Instead, these further attest that the performance of the composite film is predominantly ruled by the quality of CIS/In_2O_3 deposition on the TNT arrays, as discussed above.

The feasibility of pulsed-electrodeposition to construct CIS-In_2O_3-TNT heterojunction electrodes comprising entire n-type components has been demonstrated in this study with detailed characterization of the crystal structure, morphological and optical properties of the materials. In particular, the introduction of CIS/In_2O_3 nanoparticles onto the surface of TNT1 array with a nanotube length of 3.3 μm was found to have the optimum photocurrent response attributing to its preeminent CIS/In_2O_3 deposition quality (i.e., homogeneously coated on the nanotubes wall while preserving the hollow structure) under the specific experimental conditions of alternating cathodic pulse at −2 V for 200 ms and short-circuit pulse at 0 V for 200 ms. Considering that photochemical stability as the main bottleneck in the application of sulfide materials, the photoelectrochemical water splitting performance of the best-performing CIS-In_2O_3-TNT1 film under visible light ($\lambda \geq 435$ nm) was then investigated *via* a two-electrode system (in a H-shaped photoelectrochemical cell with the anode and cathode chambers partitioned using a Nafion membrane), in which Pt foil

was used as the cathode.

Both sulfide (S^{2-}) and sulfite (SO_3^{2-}) ions have been extensively demonstrated as effective reducing agents to scavenge holes from the excited sulfide anode in a photoelectrochemical cell, at which the photogenerated holes can oxidize S^{2-} into disulfide (S_2^{2-}) ions (Equation 2) and SO_3^{2-} into sulfate (SO_4^{2-}) and dithionate ($S_2O_6^{2-}$) ions (Equations 3, 4), respectively [12]. Utilization of electrolyte containing either S^{2-} or SO_3^{2-} ions is therefore useful to suppress photocorrosion of the sulfide anode. While the hole-scavenging ability of S^{2-} ions has been demonstrated to be greater than that of SO_3^{2-} ions to facilitate better production of H_2 at the cathode *via* water reduction (Equation 5) [11], the formation of yellow S_2^{2-} ions is highly undesirable because not only do they act as an optical filter that reduces the light absorption of the photoelectrode, they also compete with proton (H^+) reduction at the cathode according to Equation 6 [12]. The increasing formation of S_2^{2-} ions during the course of reaction would therefore deteriorate the rate of H_2 production. Addition of SO_3^{2-} ions into the S^{2-} solution is shown to efficaciously suppress the formation of S_2^{2-} ions, whereby S_2^{2-} as the oxidation product of S^{2-} can further react with SO_3^{2-} to yield thiosulfate ($S_2O_3^{2-}$) and S^{2-} ions (Equation 7) that absorb less UV light than the S_2^{2-} ions [12]. Therefore, the mixture of S^{2-} and SO_3^{2-} ions is considered as a better substitute for the electrolyte containing pure S^{2-} or SO_3^{2-} ions to subdue the stability issue of sulfide photoanode [13].

Hole scavenging:

$$2S^{2-} + 2h^+ \rightarrow S_2^{2-}, \quad (2)$$

$$SO_3^{2-} + 2OH^- + 2h^+ \rightarrow SO_4^{2-} + H_2O, \quad (3)$$

$$2SO_3^{2-} + 2h^+ \rightarrow S_2O_6^{2-}. \quad (4)$$

Water reduction:

$$2H_2O + 2e^- \rightarrow H_2 + 2OH^-. \quad (5)$$

Disulfide competition for electrons:

$$S_2^{2-} + 2e^- \rightarrow 2S^{2-}. \quad (6)$$

Suppression of disulfide formation:

$$S_2^{2-} + SO_3^{2-} \rightarrow S_2O_3^{2-} + S^{2-}. \quad (7)$$

However, the $\eta_{current}$ of the two-electrode photoelectrochemical water splitting system was found to maintain at merely 20% over a 4 h measurement period (as depicted in Fig. 4a) when Na_2S/Na_2SO_3 mixture was employed as the electrolyte solution in both the anode (CIS-In_2O_3-TNT1) and cathode (Pt) chambers. This indicates that only 20% of the photogenerated current is utilized in the reduction of H^+ to produce H_2. There are two main reasons for the decreased activity in H_2 generation under this condition: (a) the presence of $S_2O_3^{2-}$ ions competing with H^+ reduction and (b) the high pH of the electrolyte solution weakens the concentration of H^+ at the cathode side. When the formation of unwanted S_2^{2-} ions is inhibited by the presence of SO_3^{2-} reducing agent, the resultant $S_2O_3^{2-}$ ions may diffuse through the Nafion membrane and contend with H^+ for the photoexcited electrons, based on Equation 8. The permeation of inorganic anions through the cation-exchange membrane has been confirmed by previous reports [21,22], verifying the possibility of $S_2O_3^{2-}$ present at the cathode (Pt) side. This then leads to the regeneration of S^{2-} and SO_3^{2-} ions accompanied with a decreased amount of electrons that can be utilized for the reduction of protons, indicating that part of the anodic photocurrent is consumed by $S_2O_3^{2-}$ *via* a reduction process. A deteriorating rate of H_2 production associated with competition of electrons between the H^+ and $S_2O_3^{2-}$ ions has been reported [12]. On the other hand, the pH of the Na_2S/Na_2SO_3 mixture electrolyte solution was measured to be at pH 12 attributing to the dissolution of Na_2S in water to produce OH^- and HS^- ions (Equation 9). At this high pH, the low $\eta_{current}$ is expected due to the low concentration of H^+. Since H^+ ions are vital in the production of H_2, the low concentration of H^+ directly impacts the amount of H_2 that can be generated on the cathode.

Thiosulfate competition for electrons:

$$S_2O_3^{2-} + 2e^- \rightarrow S^{2-} + SO_3^{2-}, \quad (8)$$

$$S^{2-} + H_2O \leftrightarrow HS^- + OH^-. \quad (9)$$

The influence of pH on the $\eta_{current}$ was investigated by employing Na_2SO_4 (pH ≈ 7) as the study electrolyte in both the anode and cathode chambers. Interestingly, the $\eta_{current}$ of the system using neutral Na_2SO_4 electrolyte solution was observed to be close to 100%, indicating that all the photoexcited electrons withdrawn from the photoanode could be utilized in H^+ reduction to form H_2. Despite the high $\eta_{current}$ achieved, the stability of the photoanode was compromised in the Na_2SO_4 electrolyte solution. Since water molecules are not as efficient as the S^{2-} and SO_3^{2-} electron donors, they do not efficiently capture the photogenerated holes and hence result in photocorrosion of the CIS-In_2O_3-TNT1. The instability of the CIS-In_2O_3-TNT1 electrode is evidently reflected in Fig. 4b by the rapid decay of the photoresponse, where only 20% of the original photocurrent maintains after a merely 2 h of visible light illumination.

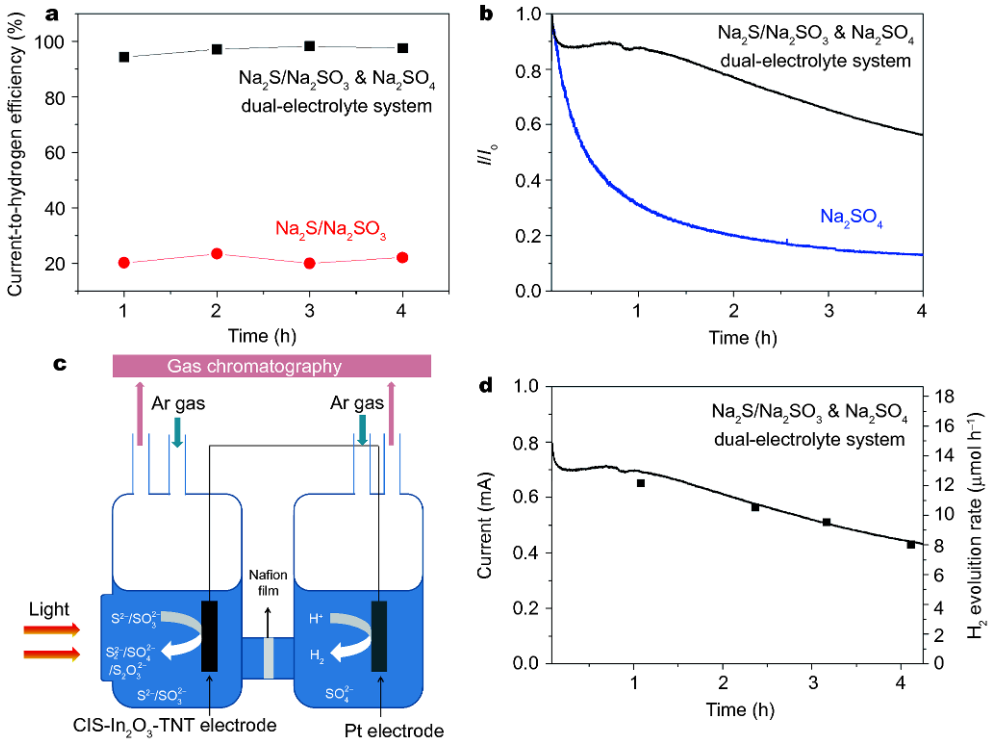

Figure 4 (a) Current-to-hydrogen efficiency of CIS-In_2O_3-TNT1 array in Na_2S/Na_2SO_3 & Na_2SO_4 dual electrolyte and Na_2S/Na_2SO_3 electrolyte in a two-electrode photoelectrochemical water splitting system for H_2 generation, (b) photocurrent of CIS-In_2O_3-TNT1 array in Na_2S/Na_2SO_3 & Na_2SO_4 dual electrolyte system and Na_2SO_4 electrolyte, (c) schematic diagram of the photoelectrochemical H_2 generation reactor featuring dual-electrolyte system and (d) photoelectrochemical H_2 evolution of CIS-In_2O_3-TNT1 array in Na_2S/Na_2SO_3 & Na_2SO_4 dual-electrolyte system.

On the basis of the requirements of Na_2S/Na_2SO_3 electrolyte to stabilize the CIS-In_2O_3-TNT1 photoanode and lower pH at the cathode to promote higher $\eta_{current}$, we develop a dual-electrolyte system to simultaneously target the stability issue of the photoanode, while achieving close to 100% $\eta_{current}$ of the water splitting system. Fig. 4c schematically illustrates the setup of the said dual-electrolyte system, whereby the chamber containing the CIS-In_2O_3-TNT1 film (anode) is filled with Na_2S/Na_2SO_3 electrolyte solution, whereas neutral Na_2SO_4 solution is used as the electrolyte in the cathode chamber accommodating the Pt foil. Fig. 4d shows the magnitude of photogenerated current in conjunction with the H_2 evolution rate for such a dual-electrolyte system under visible light illumination. While the photocurrent stability was shown to be improved by sustaining 60% of the original photocurrent after 4 h of visible light illumination (Fig. 4b), the $\eta_{current}$ of the system was also found to concurrently enhanced to close to 100% (Fig. 4a). These results show that while utilization of Na_2S/Na_2SO_3 mixture effectively consumes the photogenerated holes from CIS-In_2O_3-TNT1 and suppresses photocorrosion of the material, employment of Na_2SO_4 electrolyte strengthens the concentration of H^+ at the cathode to expedite electron consumption for H_2 generation.

CONCLUSIONS

Heterojunction photoanode comprising n-type CIS and In_2O_3 nanoparticles electrochemically deposited on n-type TNT array was produced *via* pulse-assisted electrodeposition approach in In-rich CIS precursor solution. Under identical electrodeposition parameters, the deposition quality of CIS/In_2O_3 on the TNT array is dependent on the TNT length; longer TNT length stimulates deposition of CIS/In_2O_3 on top of the TNT array and the subsequent tube closure. The unambiguously higher photocurrent of the CIS-In_2O_3-TNT composite film with homogenous deposition of CIS/In_2O_3 on the TNT surface without sealing the nanotubes (CIS-In_2O_3-TNT1) in comparison to the films composed of sealed TNT arrays by the formation of a dense CIS/In_2O_3 top layer (CIS-In_2O_3-TNT3 and CIS-In_2O_3-TNT7) substantiates the crucial role of hollow TNT as the light scattering centers to enhance the charge generation and

separation of the composite electrode. Introduction of a dual-electrolyte water splitting system, in which the CIS-In_2O_3-TNT photoanode was immersed in Na_2S/Na_2SO_3 electrolyte solution while the Pt cathode in pH-neutral Na_2SO_4 solution was demonstrated to enhance the anode photostability and concomitantly boost the $\eta_{current}$ of the system to close to 100%, as opposed to the merely 20% $\eta_{current}$ in system utilizing Na_2S/Na_2SO_3 as the single-electrolyte in both anode and cathode chambers. Such a dual-electrolyte system sheds light on the practicability of using two different electrolytes in a photoelectrochemical water splitting cell to simultaneously target the photochemical instability issue of the electrode and improve the overall $\eta_{current}$ of the system. This paves a new avenue in the design of advanced photoelectrochemical system consisting of small bandgap yet photochemically unstable catalyst, particularly the sulfide materials.

Received 7 November 2017; accepted 26 February 2018; published online 4 April 2018

1 Fujishima A, Honda K. Electrochemical photolysis of water at a semiconductor electrode. Nature, 1972, 238: 37–38
2 Guo J, Zhou H, Ouyang S, *et al.* An Ag_3PO_4/nitridized Sr_2 Nb_2O_7 composite photocatalyst with adjustable band structures for efficient elimination of gaseous organic pollutants under visible light irradiation. Nanoscale, 2014, 6: 7303–7311
3 Yun JH, Ng YH, Huang S, *et al.* Wrapping the walls of n-TiO_2 nanotubes with p-$CuInS_2$ nanoparticles using pulsed-electrodeposition for improved heterojunction photoelectrodes. Chem Commun, 2011, 47: 11288–11290
4 Fujishima A, Rao TN, Tryk DA. Titanium dioxide photocatalysis. J Photochem Photobiol C-Photochem Rev, 2000, 1: 1–21
5 Wang H, You T, Shi W, *et al.* Au/TiO_2/Au as a plasmonic coupling photocatalyst. J Phys Chem C, 2012, 116: 6490–6494
6 Tang Y, Traveerungroj P, Tan HL, *et al.* Scaffolding an ultrathin CdS layer on a ZnO nanorod array using pulsed electrodeposition for improved photocharge transport under visible light illumination. J Mater Chem A, 2015, 3: 19582–19587
7 Selloni A. Anatase shows its reactive side. Nat Mater, 2008, 7: 613–615
8 Pan J, Liu G, Lu GQM, *et al.* On the true photoreactivity order of {001}, {010}, and {101} facets of anatase TiO_2 crystals. Angew Chem Int Ed, 2011, 50: 2133–2137
9 Kazmerski LL, Ayyagari MS, Sanborn GA. $CuInS_2$ thin films: Preparation and properties. J Appl Phys, 1975, 46: 4865–4869
10 Tang Y, Wang P, Yun JH, *et al.* Frequency-regulated pulsed electrodeposition of $CuInS_2$ on ZnO nanorod arrays as visible light photoanodes. J Mater Chem A, 2015, 3: 15876–15881
11 Minoura H, Tsuiki M. Anodic reactions of several reducing agents on illuminated cadmium sulfide electrode. Electrochim Acta, 1978, 23: 1377–1382
12 Reber JF, Meier K. Photochemical production of hydrogen with zinc sulfide suspensions. J Phys Chem, 1984, 88: 5903–5913
13 Buehler N, Meier K, Reber JF. Photochemical hydrogen production with cadmium sulfide suspensions. J Phys Chem, 1984, 88: 3261–3268
14 Yun JH, Ng YH, Ye C, *et al.* Sodium fluoride-assisted modulation of anodized TiO_2 nanotube for dye-sensitized solar cells application. ACS Appl Mater Interfaces, 2011, 3: 1585–1593
15 Boiko M, Medvedkin G. Thermal oxidation of $CuInSe_2$: Experiment and physico-chemical model. Sol Energy Mater Sol Cells, 1996, 41-42: 307–314
16 Dirnstorfer I, Hofmann DM, Meister D, *et al.* Postgrowth thermal treatment of CuIn(Ga)Se_2: Characterization of doping levels in In-rich thin films. J Appl Phys, 1999, 85: 1423–1428
17 Asenjo B, Chaparro AM, Gutiérrez MT, *et al.* Quartz crystal microbalance study of the growth of indium(III) sulphide films from a chemical solution. Electrochim Acta, 2004, 49: 737–744
18 Shankar K, Bandara J, Paulose M, *et al.* Highly efficient solar cells using TiO_2 nanotube arrays sensitized with a donor-antenna dye. Nano Lett, 2008, 8: 1654–1659
19 Jiang Z, Tang Y, Tay Q, *et al.* Understanding the role of nanostructures for efficient hydrogen generation on immobilized photocatalysts. Adv Energy Mater, 2013, 3: 1368–1380
20 Ma Y. Synthesis of TiO_2 nanotubes film and its light scattering property. Chin Sci Bull, 2005, 50: 1985
21 Unnikrishnan EK, Kumar SD, Maiti B. Permeation of inorganic anions through Nafion ionomer membrane. J Membrane Sci, 1997, 137: 133–137
22 Danielsson LG, Yang X. Transport of low molecular weight anions through a Nafion ionomer membrane: application to kraft cooking liquors. Anal Chem, 2000, 72: 1564–1568

Acknowledgements This work was supported by the Australian Research Council (DP170102895). We thank the UNSW Mark Wainwright Analytical Centre for providing access to all analytical facilities.

Author contributions Ng C and Yun JH fabricated the electrodes and conducted the photoelectrochemical measurements. Tan HL and Wu H performed characterizations on the samples. Amal R and Ng YH supervised this work. All authors analyzed the data and completed the paper.

Conflict of interest The authors declare no conflict of interest.

Charlene Ng is currently an Alexander von Humboldt Postdoctoral Fellow at Leibniz-Institut für Polymerforschung Dresden. She received her PhD in Chemical Engineering from UNSW Australia and was awarded for a 3-year OCE Postdoctoral Fellowship from Year 2014–2017 at the Commonwealth Scientific and Industrial Research Organization in Melbourne, Australia. Her primary research interests are aimed at addressing challenges associated with the conversion of solar energy into chemical fuels.

Yun Hau Ng received his PhD from Osaka University in 2009. After a brief research visit to the University of Notre Dame, he joined UNSW with the Australian Postdoctoral Fellowship (APD) in 2011. He is currently a senior lecturer in the School of Chemical Engineering at UNSW. His research is focused on the development of novel photoactive semiconductors (particles and thin films) for solar energy conversion.

$CuInS_2$-In_2O_3-TiO_2纳米管阵列薄膜双电介质体系在光电化学产氢中的应用

Charlene Ng, Jung -Ho Yun, Hui Ling Tan, Hao Wu, Rose Amal, Yun Hau Ng*

摘要 光电化学电池产氢过程中利用Na_2S/Na_2SO_3混合物作为电解质溶液稳定硫化物阳极通常会牺牲电流产氢效率($\eta_{current}$). 本文采用Na_2S/Na_2SO_3和pH中性的Na_2SO_4分别作为光解水电池的阳极和阴极电解液可有效抑制$CuInS_2$-In_2O_3-TiO_2 (CIS-In_2O_3-TNT)纳米管杂化结构的光腐蚀, 同时提高$\eta_{current}$. 通过脉冲辅助电沉积法可将n型CIS和In_2O_3纳米粒子沉积在TNT阵列表面, 在保留TNT原有中空结构的前提下将纳米粒子均匀沉积在纳米管上对于在杂化结构中获得高效电荷聚集和分离非常必要. 与Na_2S/Na_2SO_3单电解液电池相比双电解液的引入不仅提高了CIS-In_2O_3-TNT阳极的光稳定性, 而且$\eta_{current}$接近于1并远高于单电解液电池(20%).

